SURFACE OXIDATION—REDUCTION KINETICS ASSOCIATED WITH EXPERIMENTAL BASALT—WATER REACTION AT 25°C

ART F. WHITE, ANDY YEE and STEVE FLEXSER

Lawrence Berkeley Laboratory, University of California, Berkeley, CA 94720 (U.S.A.)

(Accepted for publication July 16, 1984)

Abstract

White, A.F., Yee, A. and Flexser, S., 1985. Surface oxidation—reduction kinetics associated with experimental basalt—water reaction at 25°C. In: Y. Kitano (Guest-Editor), Water—Rock Interaction. Chem. Geol., 49: 73—86.

Distributions of Fe(II) and Fe(III) during basalt—water interaction at 25°C were experimentally investigated under open- and closed-system conditions relative to O_2 and CO_2. After reaction, X-ray photoelectron spectroscopy analyses detected oxidized Fe on the surface of basalt, the concentration of which decreased as a function of reaction pH. Concurrent increases in Fe(II) and decreases in Fe(III) in solutions at pH's < 5 indicated continued surface oxidation by the reaction:

$$(Fe(II)\tfrac{1}{z}M^z)_{basalt} + Fe(III)_{solution} \rightarrow Fe(III)_{basalt} + Fe(II)_{solution} + \tfrac{1}{z}M^z{}_{solution}$$
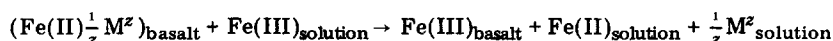
where the electrical charge in solution is balanced by dissolution of a cation of charge z from the basalt.

At neutral to basic pH, Fe(II) is oxidized to Fe(III) and precipitated as ferric oxyhydroxide in the presence of O_2. Fe(II) is also strongly sorbed on the basalt surface, resulting in low aqueous concentrations even under anoxic conditions. The rate of O_2 uptake increased with decreasing pH. Diffusion coefficients of the order 10^{-14} cm^2 s^{-1}, calculated using a one-dimensional diffusion model, suggest grain boundary diffusion in Fe-oxides.

1. Introduction

Weathering of primary Fe-silicates and Fe-oxides in an aquifer may have a strong impact on aqueous speciation and on the rates of chemical migration. Aside from acting as a major source term for the cycling of Fe, such weathering may also affect aqueous oxidation—reduction reactions, dissolved oxygen concentrations and the formation of secondary Fe-oxyhydroxides.

High concentrations of electroactive Fe at low pH have been shown to control the overall Eh of geochemical systems such as in mine drainages (Nordstrom et al., 1979). The effects of Fe speciation on the Eh of neutral to alkaline pH groundwaters are not well understood in part due to generally low dissolved Fe concentrations. However, such aquifers have generally been considered devoid of dissolved oxygen (D.O.) because of oxidation of Fe-containing minerals. Recent data (Winograd and Robertson, 1982), showing appreciable dissolved oxygen in several old groundwater systems, may require re-evaluation of kinetic processes associated with Fe oxidation.

Finally, transport of chemical species, in-

cluding trace metals and radionuclides has been shown to be strongly retarded by sorption and coprecipitation with Fe-oxyhydroxides (Hilderbrande and Blume, 1974). Based on decreased dissolution rates in oxygenated solutions, Siever and Woodford (1979) proposed that Fe-containing rocks, such as basalt, become armored with oxyhydroxide precipitates. Such coatings could process extremely large surface areas and effectively sorb cationic species from solution. However, data on naturally weathered amphiboles and pyroxenes (Berner and Schott, 1982) found no increases in surface Fe. Additional data are needed on the effects of weathering of primarily Fe-containing minerals on rates and morphology of Fe-oxyhydroxide precipitation.

The purpose of the present investigation of basalt, as well as other ongoing work on individual Fe-silicate minerals, is to define the mechanisms and kinetics of oxidation—reduction reactions associated with rock—water interaction. Basalt was chosen in this study because it is the most common rock containing high Fe concentrations. The basalt of the Columbia Plateau, Washington, U.S.A., is particularly significant in terms of groundwater interaction because it is a candidate site for emplacement of high-level nuclear waste. The type of chemical processes outlined above may have a significant impact on potential radionuclide migration.

2. Mineralogy

The Grande Ronde basalt (6—16 Myr. B.P.) comprises ~70% of the total basalt accumulation of the Pasco basin, south-central Washington, U.S.A. (Meyers and Price, 1979). Samples of two units, the Umtanum and the Cohassett, were used in this study. The overall bulk chemistries of these units are presented in Table I. Although total Fe is very similar in the two flow units, Fe(III) is higher in the Umtanum basalt possibly due to greater high-temperature oxidation of Fe-oxides (Haggerty, 1976).

TABLE I

Chemical analyses (wt.%) of Columbia Plateau basalt

	Cohassett flow of the Grande Ronde Formation	Umtanum flow of the Grande Ronde Formation
SiO_2	53.41	54.90
TiO_2	1.79	2.17
Al_2O_3	15.00	14.34
Fe_2O_3	4.36	4.81
FeO	9.42	8.71
MnO	0.20	0.22
MgO	4.99	3.48
CaO	8.86	7.30
Na_2O	2.82	2.66
K_2O	1.00	1.48
P_2O_5	0.27	0.35
Total	102.12	100.42

The mineralogy of the Umtanum flow is characterized by Noonan (1980). Dominant Fe-silicates in the Umtanum flow include augite (20—45 wt.%) and pigeonite (1—10 wt.%) and relatively rare olivine (0—3 wt.%). Titaniferous magnetite is the dominant Fe-oxide (0—7 wt.%), occurring as dendritic or coarsely crystalline grains. An interstitial glassy groundmass or mesotasis (15—70 wt.%) is abundant.

Petrographic and microprobe characterizations of the Cohassett flow were performed in the current study due to a lack of previously published data. Plagioclase (labradorite), augite, and rarely olivine occur as phenocrysts in the Cohassett samples, and plagioclase and augite occur as groundmass phases as well. Typical compositions of these phases are given in Table II. Groundmass plagioclase appears to be a distinct phase (andesine), more sodic than the phenocryst composition shown in Table II. Augite spans a range in composition; groundmass augite is generally higher in FeO (to 17—19% FeO) and lower in MgO (to 13—11% MgO) than the average given in Table II. Olivine occurs as remnants of larger grains now almost entirely altered to a clay mineral.

TABLE II

Microprobe analysis of Fe-containing mineral phases in the Cohassett basalt

	Number of analyzed points, n	SiO_2	TiO_2	Al_2O_3	FeO(*1)	MgO	CaO	Na_2O	K_2O	Total
Plagioclase (phenocrysts)	46	53.05 ± 1.0*2	0.09 ± 0.09	27.79 ± 0.62	0.66 ± 0.15	0.21 ± 0.1	11.93 ± 0.3	4.25 ± 0.5	0.26 ± 0.04	98.2
Augite	42	50.16 ± 0.92	1.36 ± 0.51	2.36 ± 0.55	12.81 ± 2.6	15.52 ± 2.2	16.38 ± 2.1	0.18 ± 0.05	—	98.8
Olivine	7	37.78 ± 1.0	0.04 ± 0.04	0.24 ± 0.3	31.09 ± 1.7	30.76 ± 2.5	0.43 ± 0.1	—	—	100.3
Titaniferous magnetite	7	1.36 ± 0.13	25.06 ± 0.52	1.79 ± 0.11	68.30 ± 0.31	0.40 ± 0.04	0.49 ± 0.04	—	0.06 ± 0.02	97.5
Glass	64	65.92 ± 1.7	0.92 ± 0.24	12.96 ± 0.95	5.48 ± 1.3	0.34 ± 0.20	2.90 ± 0.62	3.89 ± 0.52	3.31 ± 0.73	95.7
Vug-filling smectite	8	53.20 ± 1.5	—	1.55 ± 0.19	12.37 ± 0.49	21.39 ± 0.35	0.81 ± 0.10	0.07 ± 0.02	0.44 ± 0.05	89.8
Alteration and fracture-filling smectite	34	46.83 ± 2.2	0.03 ± 0.02	3.60 ± 0.56	17.98 ± 1.3	16.59 ± 0.85	1.14 ± 0.21	0.09 ± 0.04	0.34 ± 0.08	86.6

*1 All Fe as FeO.
*2 Error is one standard deviation (1σ).

TABLE III

Summary of selected experimental parameters

Experiment No.	Initial solution composition	Basalt (g l⁻¹)	Initial O_2 (ppm)	Initial pH	Final O_2 (ppm)	Final pH	Total time (10^5 s)
Closed system:							
1	D.I. H_2O	80	<0.20	9.63	0.80	9.15	68
2	D.I. H_2O	80	9.23	5.46	0.17	5.62	63
3	D.I. H_2O	80	<0.20	4.94	<0.20	5.58	78
4	D.I. H_2O	80	9.34	2.62	0.95	3.80	23
5	10 ppm Fe(II)	16	9.48	6.50	7.86	6.48	3.4
6	70 ppm Fe(II)	16	9.48	6.50	2.20	6.35	3.4
Open system:							
7	2 ppm Fe(III)	2.6	~9	3.46	~9	3.52	0.93
8	2 ppm Fe(III)	13.3	~9	3.42	~9	3.46	0.93
9	2 ppm Fe(III)	2.6	~9	4.48	~9	4.53	0.93
10	2 ppm Fe(III)	13.3	~9	4.02	~9	4.57	0.93

The groundmass of the Cohassett samples is composed of a dark-brown glassy matrix enclosing fine- to micro-crystalline grains of plagioclase (andesine), augite, titaniferous magnetite, glass and clay minerals. Titaniferous magnetite is a very abundant constituent of the groundmass, where it occurs as narrow cruciform grains typically 5—10 μm in

PLATE I
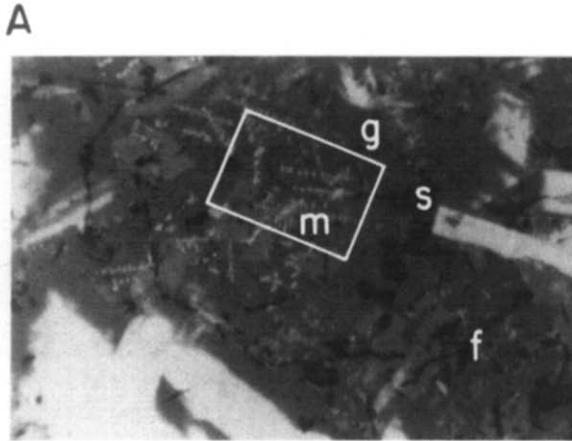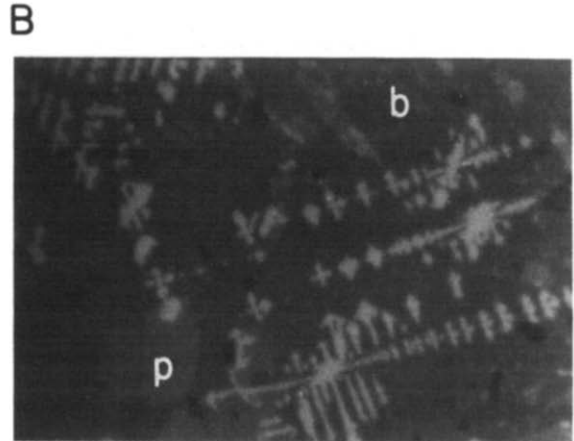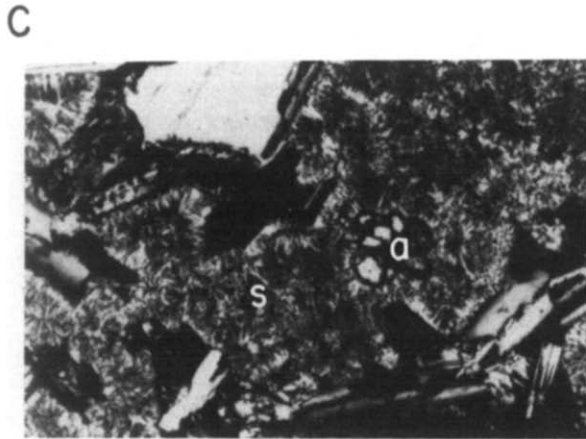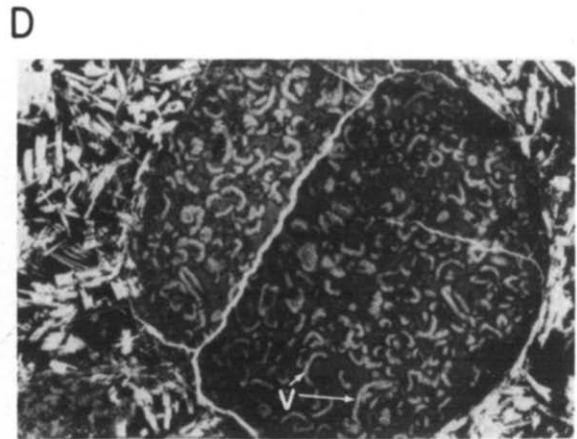
Photomicrographs of Cohassett basalt flow.

A. Glass (g), smectite alteration (s) and fracture filling (f), and titaniferous magnetite (m) in groundmass. Phenocrysts are plagioclase. Incident light.

B. Titaniferous magnetite in area outlined in (A). Groundmass plagioclase (p) and immiscible liquid blebs (b) are also visible in the glassy matrix. Incident light.

C. Fibrous smectite alteration (s) surrounding unaltered core of augite (a). Phenocrysts are mainly plagioclase. Cross-polarized transmitted light.

D. Fractured vug filling, with vermicular smectite (v) in a finer smectite matrix. Pocket of clay alteration is at lower left. Plane-polarized transmitted light.

width and up to 100 μm in length [Plate I, (B)]. Their narrow width — on the order of the electron beam diameter — made accurate microprobe determination of composition difficult. Table II shows the average of probe analyses closest to the pure phase, as judged by highest Fe and Ti counts, and lowest counts of other elements, particularly Si.

The glass in the groundmass [Plate I, (A) and (B)] is quite variable in composition, with FeO concentrations commonly ranging from 4% to 8%. Differences in glass coloration often correlate with compositional differences, with darker glass generally higher in FeO. Some areas of nearly opaque glass had FeO concentrations up to 10—15%, but these concentrations were probably due to inclusions of sub-microscopic magnetite grains. Glass immediately surrounding grains of titaniferous magnetite is usually relatively light in color, suggesting adjacent glass was depleted in FeO and did not completely homogenize after magnetite crystallization. Although the glass phase is generally low in Fe relative to several other phases in this basalt, rapid weathering of glass (White et al., 1980) may contribute significantly to overall reaction rates.

Smectite is abundant as both an alteration product and a vug and fracture-filling material. It occurs as fine orange or green needles in radial or vermicular arrays, or in finer clots of sub-microscopic crystals. Areas of extensive smectite growth are usually cut by fine shrinkage cracks, and interconnected by fractures, making them readily accessible to circulating solutions. Vug-filling smectite [Plate I, (D)] is compositionally distinct from alteration and fracture-filling smectite [Plate I, (C)] as shown in Table II. It is also more uniform in composition, and is extremely low in Al_2O_3 for a smectite mineral. However, X-ray patterns, including those of glycolated specimens, confirm a basic trioctahedral smectite structure.

3. Experimental methods

Fresh samples of the Umtanum and Cohassett flow units were obtained from drill-core and outcrop material, respectively. To avoid Fe contamination during processing, sawed slabs were buffed on an Fe-free lap, crushed with a ceramic disc mill and graded using stainless-steel sieves. The 0.42—0.18-mm size fraction was ultrasonically cleaned and fines decanted off in a O_2-free glove box. The basalt was dried and stored under high vacuum.

Experimental conditions of individual basalt—water reactions are described in Table III. Solutions were buffered by using different ratios of $NaHCO_3$, HCl and dissolved CO_2. Under open-system conditions, solutions were exposed to a constant flow of O_2 and CO_2. Under closed-system conditions required to monitor O_2 uptake, atmospheric interaction was excluded. Basalt samples were added to a series of 125-ml Erlenmeyer flasks filtered with ground glass stoppers in a N_2-filled glove box. The flasks with added solutions were ultrasonically agitated to remove trapped gas and sealed with silicone grease. Analysis of O_2-free blanks, after storage for six months in air, indicated negligible O_2 contamination.

Flasks containing basalt were periodically opened and dissolved oxygen (D.O.) was measured by using an Orion® electrode (±0.05 ppm). Experiments using O_2-free solutions indicated that the minimum measurable D.O.-value was ~0.20 ppm due to O_2 contamination during introduction of the electrode into the flask. The Eh of the solution was subsequently measured by using an Orion® Pt electrode calibrated against a Zobell solution. An aqueous sample was immediately extracted by a gas-tight syringe, filtered (0.2 μm), acidified and analyzed for Fe(II) and total Fe. Other major dissolved components, including Na, K, Ca, Mg, Si and Al, were analyzed later.

Aqueous Fe was determined spectrophotometrically using a ferrozine chromagen (Gibbs, 1979) with a lower limit of detection of 10 μg l^{-1}. Because ferrozine reacts only with the ferrous ion, the Fe(II)/Fe(III) ratio in solution was conveniently determined by reducing a sample split with hydroxylamine, measuring total Fe, and calculating Fe(III) by the difference relative to Fe(II).

Ferrous—ferric iron in the bulk basalt samples (Table I) was also determined from Fe(II) and total Fe. Ferrous iron was analyzed by dissolving the basalt in a HF solution containing V(V) which oxidized Fe(II) as it dissolved into solution (Wilson, 1955). Fe(II) was determined by titration of excess V(V). Total Fe was determined in the HF solution by atomic absorption spectrometry.

The Fe concentration and oxidation states on the composite surfaces of basalt mineral grains were determined using X-ray photoelectron spectroscopy (XPS). The theory, instrumentation and application of XPS to geological studies have been reviewed by Bancroft et al. (1979) and applied to Fe-silicates by Berner and Schott (1982). The technique involves irradiation of the solid surface in vacuo with monoenergetic soft X-rays and sorting the emitted electrons by energy. Since the mean free path of the electrons is very small, the electrons which are detected originate from only the top few atomic layers (~ 20 Å). In this study, the basalt surface chemistry was investigated by using a Physical Electronics® multiprobe with a Mg X-ray source.

4. Results

4.1. Iron release from basalt

Release of chemical species into solution during experimental dissolution of basalt was found to be highly incongruent as shown for Umtanum basalt in Fig. 1. Relatively rapid release of Na and Si, common for glassy rocks (White et al., 1980), suggests preferential dissolution of the alkali-silica-rich mesotasis. Dissolution rates become linear at longer reaction times.

As indicated by dissolution data in Fig. 2, aqueous Fe concentrations are strongly pH dependent. At moderately acidic pH, the dominant Fe(II) species increase initially with time and then level off in a pattern similar to that reported for basalt by Siever and Woodford (1979). Dissolution data for Fe do not appear to fit any simple linear or parabolic
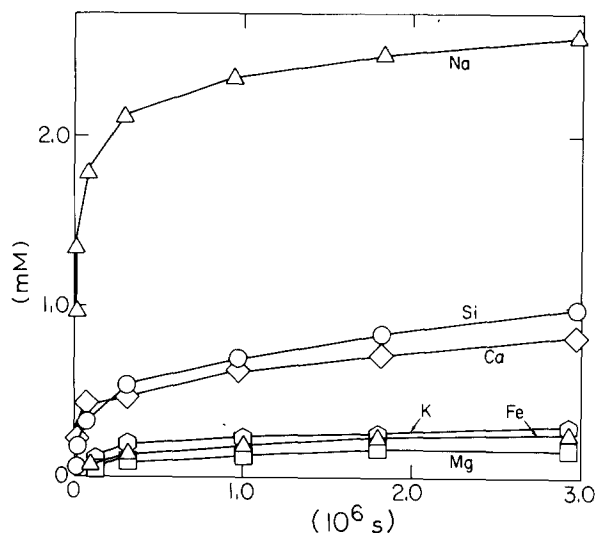

Fig. 1. Release of major chemical species during weathering of Umtanum basalt over 75 days at an average pH of 5.5 (experiment 2, Table III).
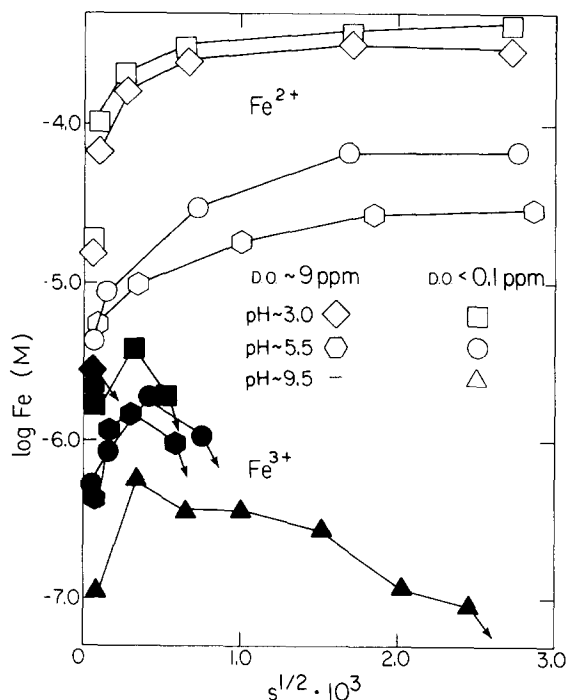

Fig. 2. Fe(II) and Fe(III) concentrations in solutions during weathering of Umtanum basalt. *Open* and *solid points* are Fe(II) and Fe(III), respectively.

rate law. Fig. 2 shows that the rate of Fe(II) release is only slightly faster at low P_{O_2} than at high P_{O_2}. No detectable Fe(II) was found in solutions below pH 7.0. Fe(III) concentrations, low over the entire pH range, initially increased in solution and then decreased below detection limits at longer times. As shown in Fig. 2, detection limits are higher at lower pH since Fe(III) is calculated from the difference between relatively large but similar concentrations of both total Fe and Fe(II). Calculation of saturation states using the WATEQF speciation code (Plummer et al., 1976) indicates that above a pH of 5.5 Fe(III) concentrations are generally supersaturated with respect to amorphous iron hydroxide Fe(OH)$_3$. Declines in aqueous concentrations in this pH range may be due to onset of such oxyhydroxide precipitation.

As indicated in Table I, appreciable Fe(III) is contained in the basalt phase assemblage as well as on the mineral surfaces. The absence of Fe(III) in solution at low pH implies either that the dissolution of Fe from basalt is highly incongruent, i.e. Fe(II) is released and Fe(III) is retained in the mineral assemblage, or that Fe(III) is being either reduced or removed from solution by some other process.

4.2. Surface chemistry

Surface compositions and Fe oxidation states were characterized by XPS. Typical spectra for Fe $2p_{1/2}$ and $2p_{3/4}$ peaks are shown in Fig. 3 for fresh and reacted Umtanum basalt. As indicated, progressive decreases in peak intensities occur with decreasing pH of reaction.

The electron binding energies of the spectral peaks can be used to estimate the surface oxidation state of Fe provided that corrections are made for surface charging. Table IV lists measured binding energies and corrected energies based on charging shifts of the adventitious carbon 1s peak from a standard state of 284.6 eV (Wagner et al., 1979). The average shift of 2.6 eV in the $2p_{3/2}$ Fe peak, due to charging, is shown in Fig. 3. Corrected binding energies for the $2p_{3/2}$ peak correspond closely to Fe(III) reported in Fe$_2$O$_3$ (712.0–712.2 eV; Allen et al., 1974; McIntyre and
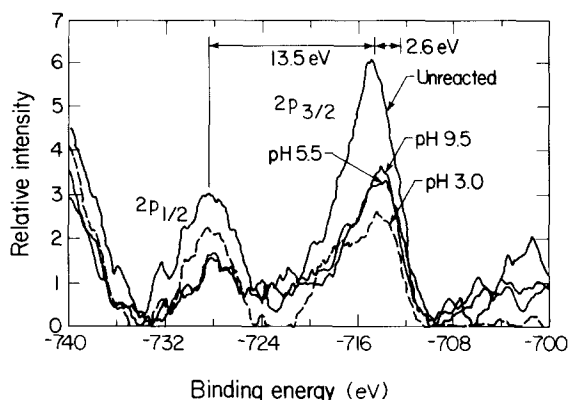

Fig. 3. XPS spectra for $2p_{1/2}$ and $2p_{3/2}$ Fe peaks showing decrease in intensity with decrease in reaction pH. An average 2.6-eV shift is due to surface charging.

TABLE IV

Measured and corrected peak positions for iron based on observed shifts in carbon spectra

Experiment No.	$C_{1s(measured)} - C_{1s(284.6\,eV)}$	Fe$_{2p_{3/2}}$	
		measured	corrected
Blank	2.60	714.9	712.3
1	2.60	714.7	712.1
2	2.80	714.1	711.3
3	2.70	714.5	711.8
4	2.50	714.7	712.2
5	2.60	714.5	711.9
6	2.60	714.0	711.4

Zetaruk, 1977), but are higher than Fe(II) in FeO (709.3 eV). The binding energy separation of 13.5 eV (Fig. 3) also agrees with that reported by Wagner et al. (1979). The quantitative atomic percentage, C_x, for a given element relative to other surface species can be obtained from data of the type shown in Fig. 3 by the relationship:

$$C_x = \frac{A_x/S_x}{\sum_i A_i \Big/ S_i} \qquad (1)$$

where A and S are the respective peak areas and atomic sensitivity factors. S_x is a function of atomic cross-sections and spectrometer detection efficiencies. Available S_x-values (Wagner et al., 1979) are based on elemental standards and may exhibit deviations for species contained in complex chemical matrix such as a silicate. To overcome such effects, elemental concentrations are often reported as ratios relative to a dominant element such as Si (Bancroft et al., 1979; Berner and Schott, 1982). Data are plotted in Fig. 4 as functions of C_x vs. pH with the atomic ratios for Fe/Si given in parentheses. A close correlation exists between the surface Fe percentage, calculated by eq. 1 for the fresh basalt, and the mole fraction contained in the bulk basalt (Table I). This correlation, in addition to the agreement between relative Fe/Si ratios, justifies the use of S_x-values in quantitative estimates of surface Fe concentrations in basalt.

As suggested by the decreases in spectral intensities in Fig. 4, decreasing reaction pH produces a quantitative drop in surface Fe concentrations in Fig. 5. At a pH of 3.5, half of the total Fe has been removed from the basalt surface. Fe decreases, particularly at high pH, indicating that Fe-oxyhydroxide coatings do not form on experimentally weathered basalt as postulated by Siever and Woodford (1979).

The effect of oxyhydroxide precipitation from solution on the surface chemistry of basalt was investigated by the addition of Fe(II) to solutions at neutral pH. As indicated in Fig. 4, resulting oxyhydroxide precipitation from a 70 ppm Fe(II) solution doubled the surface Fe concentration while precipitation from a 10 ppm Fe(II) solution failed to increase the surface concentration to a level initially present on the unreacted basalt. The initial Fe(II) solutions were also tagged with 0.1 mM CsCl$_2$ and 0.1 mM SrCl$_2$ to determine if coprecipitation or sorption occurred in oxyhydroxide phases on the basalt surface. In all cases, the $3d_{5/2}$ peaks for Cs and Sr were found to be below XPS sensitivity levels. The above results suggest that Fe-oxyhydroxides form by homogeneous nucleation in solution rather than as surface coatings on Fe-silicate grains, a conclusion supported by visual inspection of suspended oxyhydroxide phases in solution.
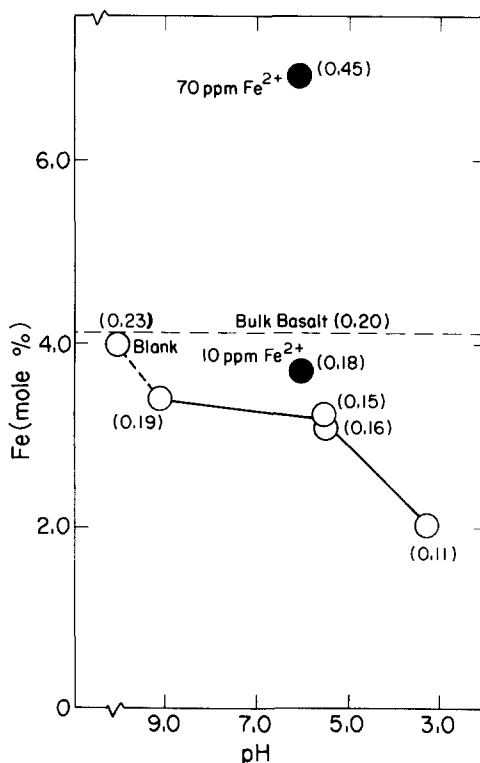

Fig. 4. Atomic percentages of Fe on the basalt surface as a function of pH. *Closed circles* are compositions resulting from addition of aqueous Fe(II). *Numbers in parentheses* are Fe/Si ratios.

4.3. Oxidation—reduction in solution

As previously indicated, at low pH Fe(III) is absent in solutions reacting with a basalt phase assemblage with significant surface and bulk Fe(III). To determine the fate of Fe(III), initial solutions containing 2 ppm Fe(III) were prepared (experiments 7—10, Table III). As shown in Fig. 5, Fe(III) is stable in blank solutions at pH's 3.0 and 4.0, indicating no reduction to Fe(II) nor precipitation as an oxyhydroxide. However, addition of Cohassett basalt decreased Fe(III) in solution at a rate proportional to pH and the basalt surface area. During the same time interval, concentrations of Fe(II) showed significant increases. At pH 3.0, the final Fe(II) concentration greatly exceeded the initial Fe(III) concentration, indicating an Fe contribution from basalt dissolution (Fig. 2). At pH 4.0 the total Fe in solution remained nearly constant over time.

One obvious explanation for the Fe(III) decrease and Fe(II) increase is that Fe^{3+} is being reduced to Fe^{2+} in solution in the presence of basalt. However, the possibility exists that corresponding changes are simply coincidental, i.e. that all of the Fe(II) is contributed from the basalt and Fe(III) is being lost by an independent mechanism such as basalt-induced precipitation or sorption. In order to uniquely define the mechanism, aqueous ^{59}Fe(III) was used as a radioactive tracer. If Fe(III) was totally reduced to Fe^{2+} in solution, the count rate should remain constant with time. If the original Fe(III) was incorporated into a solid phase the count rate should approach zero in solution. As shown in Fig. 5C, ^{59}Fe concentrations do decrease with time with increasing pH and basalt surface areas. However, the ^{59}Fe decrease is less and the rates much slower than that of Fe(III), indicating that significant reduction of Fe must occur in solution.
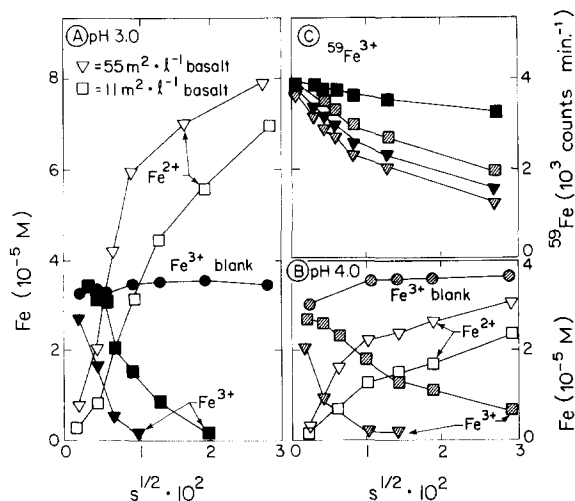
At pH's greater than 6.0, Fe(II) is rapidly depleted in solution, as indicated by the lack of measurable Fe(II) in the basalt dissolution studies (Fig. 2). Fe concentrations in this pH range are controlled by the precipitation of oxyhydroxides:

$$Fe^{2+} + \tfrac{1}{4}O_2 + 2OH^- + \tfrac{1}{2}H_2O \rightarrow$$

$$Fe(OH)_3 \qquad\qquad (2)$$
amorphous hydroxide

$$Fe^{2+} + \tfrac{1}{4}O_2 + 2OH^- \rightarrow \tfrac{1}{2}H_2O + FeO(OH) \qquad (3)$$
goethite
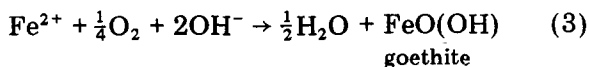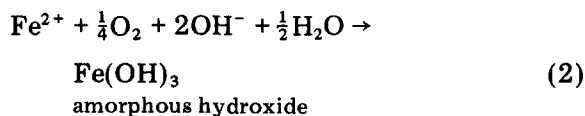
A number of studies (Stumm and Lee, 1961; Pankow and Morgan, 1981; Davison and Seed, 1983) have shown that Fe(II) oxidation kinetics obey the rate law:

$$d[Fe(II)]/dt = k[Fe(II)]P_{O_2}(OH^-)^2 \qquad (4)$$

where [Fe(II)] is the measured concentration (M); P_{O_2} is the partial pressure of oxygen (atm.); and OH^- is the activity of the hydroxyl ion. When pH and P_{O_2} are constant, eq. 4 reduces to:

$$d[Fe(II)]/dt = k_1[Fe(II)] \qquad (5)$$

where

$$k_1 = k(OH^-)^2 P_{O_2} \qquad (6)$$

Experiments were conducted at a buffered pH of 6.5 and at atmospheric O_2 to determine

Fig. 5. Trends in Fe speciation with time in solutions initially containing 2 ppm $FeSO_4$ and varying amounts of Cohassett basalt. *Open points* are Fe(II) concentrations and *solid* and *hatched points* are Fe(III) concentrations at pH 3.0 (A) and pH 4.0 (B), respectively. ^{59}Fe(II) is plotted as counts per min. (C).

the effects of basalt interaction on oxidation kinetics of Fe(II) at near-neutral pH. As shown by the example in Fig. 6, Fe(II) oxidation rates in blank solutions display a linear relationship between log[Fe(II)] and time as predicted by eq. 5. The slope of the line, which corresponds to $k_1/2.3$, results in a rate constant (k) of $1.64 \cdot 10^{14}$ mol^{-2} atm.$^{-1}$ min.$^{-1}$ which falls within the range of rate constants summarized by Davison and Seed (1983).

The addition of basalt to solutions at near-neutral pH has the effect of greatly accelerating the Fe(II) decrease (Fig. 6). The rates become non-linear with respect to eq. 5 and proportional to the total surface area of the basalt present, suggesting uptake by the solid.
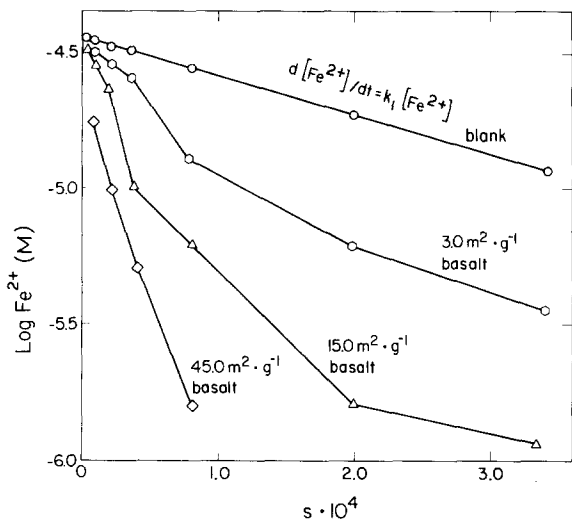

Fig. 6. Oxidation rate of Fe(II) in solution with varying basalt surface areas. Data for blank solution are fit to first-order rate law (eq. 5).

4.4. Uptake of dissolved oxygen

To test the effect of oxyhydroxide precipitation in controlling both dissolved Fe(II) and O_2 concentrations at neutral pH, blank solutions were saturated at a given P_{O_2}, Fe(II) was added, and P_{O_2} was measured after the system achieved equilibrium. As indicated in Fig. 7, the 4 : 1 ratio between total Fe(II) consumed (M) and the final dissolved O_2 con-

tent (M) reproduces the stoichiometry of reactions (2) and (3). Addition of basalt to the solutions decreases the initial Fe(II)/final P_{O_2} ratios to less than 4 : 1. This decreased slope, which is proportional to the basalt surface area, implies a loss of Fe(II) from solution which is not associated with the formation of Fe-hydroxide or goethite.

Rates of O_2 uptake were also monitored in the long-term closed-system experiments (Table III, experiments 1—4) in which the iron chemistry was controlled solely by basalt reaction. Examples of O_2 uptake are shown in Fig. 8. While short-term O_2 uptake from blank solutions containing added Fe(II) can be quantified based on the stoichiometry of reactions (2) and (3), long-term O_2 uptake in solutions containing basalt cannot be explained by the release of Fe to solution and subsequent oxyhydroxide precipitation. O_2 uptake rates increase with decreasing pH and increasing oxyhydroxide solubilities. The fastest uptake rate is observed at pH 3.0 (Fig. 8) where the aqueous Fe speciation is undersaturated
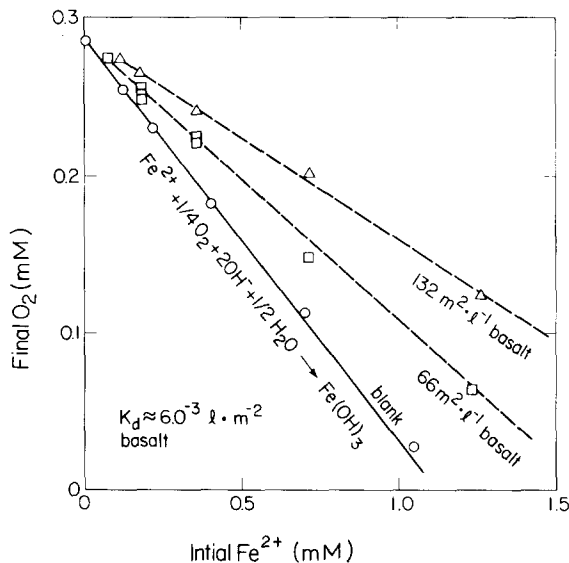

Fig. 7. Relationship between initial Fe(II) and final dissolved oxygen concentrations after equilibrium with oxyhydroxide. *Lower line* shows stoichiometric relationship for blank solution while progressive deviations with increasing basalt surface areas indicate Fe sorption as described by eq. 10.

with amorphous Fe-hydroxide. Even at higher pH's, where solutions do become saturated with $Fe(OH)_3$, the amount of Fe(III) precipitated is much less than that required to balance the rate of O_2 uptake based on the 4 : 1 stoichiometry of reactions (2) and (3). For example, total Fe(II) precipitated at pH 5.0 is estimated to be 0.2 mM based on the difference in dissolved Fe concentrations of the oxic and anoxic experiments. This Fe concentration is much less than the observed O_2 uptake of 0.2 mM at pH 5.0 (Fig. 8).

The generally parabolic decrease in oxygen with time (Fig. 8) suggests a diffusion-controlled reaction with the basalt. Rates can be modeled by assuming diffusion from a well-stirred solution of finite extent. Due to generally slow solid-state diffusion rates at ambient temperature, the basalt can be represented as an infinite one-dimensional

slab. An analytical solution to Fick's second law of diffusion with appropriate boundary conditions is presented by Carslaw and Jaeger (1959) for analogous heat diffusion. The measured O_2 concentration, C, is related to the initial O_2 concentration, C_0, by the relationship:

$$C = C_0 \exp(Dt/l)\ \text{erfc}(Dt/l) \qquad (7)$$

where D is the oxygen diffusion coefficient; and t is time in seconds. The solution length, l (cm), is the one-dimensional representation of solution volume (cm^3) divided by basalt surface area (cm^2). The dotted lines in Fig. 8 are solutions to eq. 7 fitted to the experimental data. The magnitude of the diffusion coefficients, 10^{-14} cm^2 s^{-1}, suggest relatively rapid grain boundary diffusion rather than slower solid-state O_2 diffusion based on low-temperature extrapolation of the data of Giletti and Anderson (1975).


Fig. 8. Oxygen loss in solution during basalt—water interaction at differing pH's. *Dashed lines* are fits to diffusion model assuming the indicated diffusion coefficients.
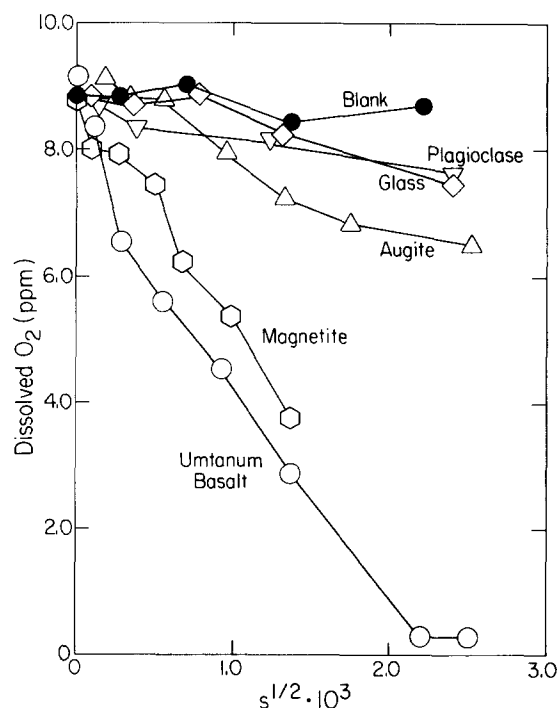

Fig. 9. Comparison of O_2 losses in solution for basalt and a number of individual silicate phases common to basalt.

Although there was no attempt in this study to assess the overall oxidation—reduction kinetics of basalt relative to individual mineral phases, it is interesting to compare O_2 uptake rates between basalt and individual mineral phases being measured in concurrent studies. Such data are plotted in Fig. 9. As indicated, rates of O_2 uptake for basalt are much faster than for silicate phases. Of particular interest is the relatively slow rate for O_2 uptake in augite, which as shown is the dominant Fe-silicate phase in basalt (Noonan, 1980). Due to lower Fe concentrations, the slow rate of O_2 uptake of obsidian glass may not be representative of the glassy mesostasis in the basalt. However, Fig. 9 clearly shows that O_2 uptake rates for basalt and magnetite are comparable, suggesting that the relatively high concentrations of titaniferous magnetite are controlling the rates of oxygen consumption.

5. Discussion and conclusions

The preceding results indicate significant interaction between the basalt mineral assemblage and dissolved Fe(II), Fe(III) and O_2 during experimental weathering. The loss of Fe from the basalt surface with decreasing pH corresponds, as expected, to an increase of Fe in the aqueous solution. In no case does an increase in surface Fe occur, indicating the absence of an oxyhydroxide coating as proposed by Siever and Woodford (1979). As indicated by XPS binding energies, reduced Fe, contained within the basalt, is oxidized on the surface of even the unreacted samples stored under atmospheric conditions. Oxidation of Fe on the surfaces of amphiboles and pyroxenes has also been demonstrated by Berner and Schott (1982).

In acidic solutions with pH's less than 5.5 and undersaturated with oxyhydroxide phases, Fe exists predominantly in the Fe(II) state. Addition of Fe(III) species results in reduction to Fe(II) in solution. Presumably Fe(III) dissolved from the oxidized basalt surface in the long-term closed-system experiments is reduced in the same manner. This

relationship, coupled with an apparent absence of other oxidizable species in solution, suggests that an oxidation—reduction couple exists between Fe(II) and Fe(III) on the basalt surface and in solution. Such a couple can be written in the form:

$$(Fe(II)\tfrac{1}{z}M^z)_{basalt} + Fe(III)_{solution} \rightarrow$$

$$Fe(III)_{basalt} + \tfrac{1}{z}M^z{}_{solution} + Fe(II)_{solution}$$

$$(8)$$
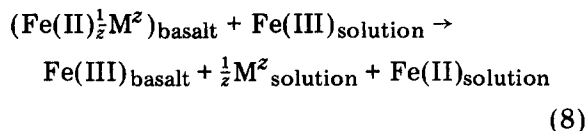
where the reduction of Fe in solution is charge-balanced by the dissolution of a cation of charge z from the basalt. As shown by the data in Fig. 1, any number of cations released into solution during experimental weathering can fulfill this requirement. The driving chemical force behind reaction (8) is apparently the continued oxidation of Fe(II) beneath the already oxidized surface of the basalt and the acceptance of electrons into solution.

At neutral to basic pH, reduction of Fe in solution by reaction (8) is countered by the oxidation of Fe during precipitation of ferric oxyhydroxides [reactions (2) and (3)]. Based on the absence of Fe(II) in solution of pH's > 5.5, the net free energy of the opposing oxidation—reduction reactions must favor oxyhydroxide precipitation over surface oxidation.

In blank solutions, kinetic rate data for Fe(II) oxidation (eq. 5), as well as closed-system oxygen uptake [reactions (2) and (3)], indicate control by oxyhydroxide precipitation. However in the presence of basalt, the rate of Fe(II) loss is accelerated and the Fe-(II): O_2 stoichiometry becomes less than that predicted by precipitation. Such deviations, coupled with observed losses of ^{59}Fe at low pH, suggest that aqueous Fe is being sorbed into the basalt surface. Such sorption can be separated from concurrent oxyhydroxide precipitation at neutral to basic pH based on deviations in final O_2 concentrations from those predicted by reactions (2) and (3). Simple sorption equilibrium can be assumed between the basalt surface and the aqueous solution:

$$[Fe(II)]_{solid} = k_d [Fe(II)]_{solution} \qquad (9)$$

The stoichiometry of reaction (2) for example can be rewritten as:

$$[Fe(II)] [1 - k_d S] + \tfrac{1}{4}O_2 + 2OH^- + \tfrac{1}{2}H_2O \rightarrow$$
$$Fe(OH)_3 \qquad (10)$$
amorphous hydroxide
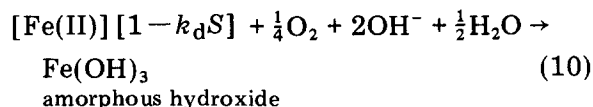
where S is the basalt surface area ($m^2 \, l^{-1}$). The dashed lines in Fig. 7 show the fits to the experimental data by using a k_d of $4.0 \cdot 10^{-3} \, l \, m^2$.

Rate data indicate that oxygen uptake increases in basalt with decreasing pH. Although oxygen is consumed by precipitation of oxyhydroxides, O_2 uptake is fastest in solutions undersaturated with such phases. Even in higher pH solutions, comparisons between rates of Fe release into oxic and anoxic solutions indicate that insufficient Fe is precipitated from the bulk solution to account for the quantities of O_2 consumed. XPS data indicate that Fe concentrations are not increasing on the exterior mineral surfaces during reaction. This information coupled with the excellent data fit to the diffusion equation suggests that oxygen continues to diffuse into interior pore spaces and along grain boundaries dominated by Fe-oxides. The reactions which consume O_2 and result in the interior diffusion gradient are not defined in this study but presumably must involve oxidation of ferrous iron and formation of a ferric oxyhydroxide. While not detected on exterior surfaces by XPS, such phases may form by heterogeneous nucleation on interior sites due to increased pH and concentration gradients.

Acknowledgements

References

Allen, G.C., Curtis, M.T., Hooper, A.J. and Tucker, P.M., 1974. X-ray photoelectron spectroscopy of iron—oxygen systems. J. Chem. Soc., Dalton Trans., p. 1526.

Bancroft, G.M., Brown, J.R. and Fyfe, W.S., 1979. Advances and applications of X-ray photoelectron spectroscopy (ESCA) in mineralogy and geochemistry. Chem. Geol., 25: 227—235.

Berner, R.A. and Schott, J., 1982. Mechanisms of pyroxene and amphibole weathering, II. Observations of soil grains. Am. J. Sci., 282: 1214—1231.

Carslaw, H.S. and Jaeger, J.C., 1959. Conduction of Heat in Solids. Oxford University Press, London, 507 pp.

Davison, W. and Seed, G., 1983. The kinetics of the oxidation of ferrous iron in synthetic and natural waters. Geochim. Cosmochim. Acta, 47: 67—79.

Gibbs, M.M., 1979. A simple method for the rapid determination of iron in natural waters. Water Res., 13: 295—297.

Giletti, B.J. and Anderson, T.F., 1975. Studies in diffusion, II. Oxygen in phlogopite mica. Earth Planet. Sci. Lett., 18: 225—233.

Haggerty, S.E., 1976. Oxidation of opaque oxides in basalt. In: Oxide Minerals Short Course Notes, Miner. Soc. Am., pp. Hg1—Hg100.

Hilderbrande, E.E. and Blume, W.E., 1974. Lead fixation by iron oxides. Naturwissenschaften, 61: 169—170.

McIntyre, N.S. and Zetaruk, D.G., 1977. Surface chemistry of iron oxides and hydroxides. Anal. Chem., 49: 1521—1524.

Meyers, C.M. and Price, S.M., 1979. Geologic studies of the Columbia Plateau: A status report. Rockwell Hanford Oper., Richland, Wash., No. RHO-BWI-ST-4.

Noonan, A.F., 1980. Phase chemistry of the Umtanum basalt: A reference repository host in the Columbia Plateau. Rockwell Hanford Oper., Richland, Wash., No. RHO-BWI-SA-77.

Nordstrom, D.K., Jenne, E.A. and Ball, J.W., 1979. Redox equilibria of iron in acid mine waters. Am. Chem. Soc. Symp. Ser., 93: 51—77.

Pankow, J.F. and Morgan, J.J., 1981. Kinetics for the aquatic environment. Environ. Sci. Technol., 15: 1155—1164.

Plummer, L.B., Jones, B.F. and Truesdell, A.H., 1976. WATEQF — a FORTRAN IV version of WATEQ, a computer program for calculating chemical equilibrium of natural waters. U.S. Geol. Surv., Water Res. Invest. No. 76-13, 61 pp.

Siever, R. and Woodford, N., 1979. Dissolution kinetics and weathering of mafic minerals. Geochim. Cosmochim. Acta, 43: 717—724.

Stumm, W. and Lee, G.F., 1961. Oxygenation of ferrous iron. Ind. Eng. Chem. 53: 143—146.

Wagner, C.D., Riggs, W.M., Davis, L.E., Mouldew, S.F. and Muilenberg, G.E., 1979. Handbook of X-ray Photoelectron Spectroscopy. Perkin-Elmer Corp., Eden Praire, Minn., 190 pp.

White, A.F., Claassen, H.C. and Benson, L.V., 1980.

The effect of dissolution of volcanic glass in the water chemistry in a tuffaceous aquifer, Rainier Mesa, Nev. U.S. Geol. Surv., Water-Supply Pap. 1535, 34 pp.

Winograd, I.J. and Robertson, F.N., 1982. Deep oxygenated ground water: anomaly or common occurrence. Science, 216: 1227—1229.

Wilson, A.D., 1955. Determination of ferrous iron in silicate minerals by a volumetric method. Bull. Geol. Soc. G.B., 9: 56—62.